Journal of Polymers and the Environment (2024) 32:94–110
https://doi.org/10.1007/s10924-023-02966-z

ORIGINAL PAPER

Fabrication and Characterization of 3D Nanostructured Polycaprolactone-Gelatin/Nanohydroxyapatite-Nanoclay Scaffolds for Bone Tissue Regeneration

Saba Nazari[1] · Mitra Naeimi[1,2] · Mohammad Rafienia[3] · Majid Monajjemi[4]

Accepted: 7 June 2023 / Published online: 10 July 2023

Abstract
Numerous clinical bone disorders, such as infections and bone loss from cancer or trauma, increase the need for bone regeneration. Due to the difficulty of self-repairing large bone defects, bone tissue engineering has gained popularity. In this study, polycaprolactone(PCL)-gelatin(GEL) scaffolds with varying concentrations of nanohydroxyapatite (NHA) and nanoclay (NC) particles were fabricated using 3D printing technology, and their physiochemical and biological properties were assessed. PCL has excellent mechanical properties, but its hydrophobicity and long-term degradation limit its utility in scaffold fabrication. Thus, GEL, NHA and NC have been used to improve the overall performance of the polymer such as hydrophilicity, strength, adhesiveness, biocompatibility, biodegradability, and osteoconductivity. The morphological analysis revealed 3D printed structures with rectangular interconnected pores and well-distributed nanoparticles. The highest porosity belonged to PCL-GEL/NHA-NC (30/70) at 69.49%, which may directly contributed to the increase in the compressive modulus and degradation rate. The wettability, compressive strength, water uptake rate, biodegradability, and bioactivity of PCL-GEL scaffolds improved significantly as the NC concentration increased. The behavior of the seeded MG-63 cells on the 3D printed nanocomposite scaffolds was evaluated using the MTT assay, DAPI staining, and SEM micro images. It was discovered that the inclusion of NHA and NC nanoparticles can promote cell proliferation, viability, and adherence. Through the obtained in vitro results, the fabricated 3D printed PCL-GEL/NHA scaffold with higher NC concentration can be regarded as a promising scaffold for expediting the repair of bone defects.

Keywords Nanohydroxyapatite nanoparticles · Nanoclay · 3D printing technology · Bone tissue engineering

Introduction

Bone is a vital organ of the body that plays an important role in body locomotion, metabolic functions, and the protection of soft structures such as the brain and lungs [1]. The skeletal system is susceptible to damage under a variety of circumstances, but it can heal itself unless the defect is large enough to necessitate intervention to accelerate osteogenesis [2]. Artificial implants and bone grafts are currently the most frequent treatment options for repairing bone abnormalities. However, previous studies have revealed that these techniques have drawbacks, including immunological rejection, limited availability, infection, and virus transmission [3].

Tissue engineering is being investigated as a promising option for bone regeneration. The primary goal of tissue engineering is to resemble tissue's native structure or to facilitate tissue formation and restore its functionality [4, 5]. One of the main pillars in tissue engineering is scaffolds.

✉ Mitra Naeimi
mit.naeimi.m@iauctb.com

✉ Mohammad Rafienia
m_rafienia@med.mui.ac.ir

[1] Department of Biomedical Engineering, Central Tehran Branch, Islamic Azad University, Tehran, Iran

[2] Medical Radiation Research Center, Central Tehran Branch, Islamic Azad University, Tehran, Iran

[3] Biosensor Research Center (BRC), Isfahan University of Medical Sciences (IUMS), Isfahan, Iran

[4] Department of Chemical Engineering, Central Tehran Branch, Islamic Azad University, Tehran, Iran

These porous structures serve as a temporary environment until the regeneration of the tissue has been completed. Depending on the desired application, scaffolds must be physically and biologically appropriate for bone repair [6]. Nowadays, in order to improve the biological and mechanical properties of the fabricated scaffolds, composite forms of them consisting synthetic and natural polymer combinations have been frequently utilized instead of using single polymers [7]. Among the synthetic polymers used in bone tissue engineering, polycaprolactone (PCL) is a semi crystalline aliphatic polyester that has excellent mechanical properties, simple processing, low melting point, and intrinsic biocompatibility [8, 9]. However, the most significant drawbacks of PCL are its hydrophobicity and long-term degradation, which limits its utility in scaffold fabrication [10]. As a result, coating or mixing PCL with a hydrophilic polymer has been used to improve the surface properties in numerous investigations [11]. Due to the semi crystalline in nature of PCL, gelatin (GEL) is a suitable choice for mixing with PCL [12]. GEL is a collagen-derived biopolymer with high molecular weight that has drawn a lot of attention because of its intrinsic properties such as hydrophilicity, high biocompatibility, biodegradability, and favorable effects on cellular activity [13]. It has also been known with its low immunogenicity and antigenicity, which effectively improves cell attachment to the scaffold and promotes cell adhesion, migration, proliferation, and differentiation [14].

Nanocomposites have been used by scientists to improve the overall performance of polymers. In this regard, significant progress has been made in the utilization of modified natural and synthetic clays for preparing polymer nanocomposites in medicine and biotechnology [15]. Nanoclays (NC) are layered silicates with a diameter of 50–200 nm which can be used with polymers to create nanocomposites that improve the polymer's stiffness, toughness and thermal properties while also enhancing swelling capability, and bio adhesion [16, 17]. All of these features point to clay's outstanding potential for fabricating novel nanocomposite scaffolds. The basic structure of bone is mineralized collagen fiber including 35% of organic matrix and 65% of minerals [10, 18]. The majority of the mineral content in bone tissue is made up of nanohydroxyapatite (NHA) structure ($Ca_{10}(PO_4)_6(OH)_2$). Bioactivity, biocompatibility, osteoconductivity, and non-corrosiveness are the most notable characteristics of NHA. As a result, it's an appealing solution for synthetic bone composite in orthopedics, dentistry, and maxillofacial surgery [19].

In designing and manufacturing of bone tissue engineering scaffolds, mechanical properties must be consistent with bone tissue [20]. The technique of constructing scaffolds is one of the approaches used to improve mechanical strength. There are a variety of scaffold fabrication methods, such as freeze drying, salt leaching, electrospinning, and gas foaming, but each has its own set of drawbacks, including non-reproducibility, inflexibility, and inhomogeneity in pore size, shape, and connectivity [21, 22]. In recent years, a novel technology based on 3D printing has been employed to fabricate scaffolds, which has resulted in major improvements in medical field due to cost savings, accuracy, and speed [23]. The technology behind 3D printing is based on patient imaging data such as CT scans and MRIs [24]. Due to complex regeneration of bone, 3D scaffolds with adequate size, porosity, cytocompability and strength and desirable cellular responses are essential to promote bone regeneration [20].

As previously mentioned, investigators have always concentrated on composites that have adequate and acceptable qualities as compared to single synthetic or natural materials. In this study, PCL, GEL, NHA, and NC has been used for creating biological scaffolds via 3D printing. The morphology, porosity percentage, compressive strength, chemical composition, hydrophilicity, bioactivity, and biodegradability of the 3D printed scaffolds were then investigated. In addition, MG-63 cells were cultured on the fabricated scaffolds, and cell growth and adhesion studies were conducted.

Materials and Methods

Materials

Polycaprolactone (PCL, Mw = 60 kDa) was supplied in the form of a 3 mm medium-sized pellets from Sigma-Aldrich (St. Louis, MO, USA). The 99.8% chloroform as PCL solvent and Bovine skin-derived gelatin (type B) was purchased from Merck (Germany). NHA nanopowder and Montmorillonite Nanoclay were obtained from Pardis Pajouhesh Fanavaran Yazd Co. (Yazd, Iran) and US Research Nanomaterials Inc. (Houston, TX, USA), respectively. Bovine fetal serum (FBS), Dulbecco's modified Eagle's medium (DMEM), Penicillin/Streptomycin, Trypsin–EDTA, phosphate buffer saline (PBS) and 3-(4,5-dimethylthiazol-2-yl)-2,5-diphenyltetrazoliumbromide (MTT) were prepared from Fisher Scientific (Mumbai, India). Glutaraldehyde solution, 4′,6-diamidino-2-phenylindole dihydrochloride (DAPI solution), simulated body fluid (SBF) and Dimethyl sulfoxide (DMSO) were supplied from Sigma-Aldrich (St. Louis, MO, USA).

Scaffold Fabrication

Ink Preparation

The PCL pellets were first dissolved in chloroform solvent for 1 h at 40 °C to attain a 50% (w/v) viscous solution for the 3D printing ink. 6.25% (w/w) GEL powder was added

Table 1 Prepared inks for 3D printing

Samples	Materials' weight ratio	Ratio of NHA-NC to PCL-GEL (W/W) (%)
S1	PCL/GEL-NHA (100%)/NC (0%)	62.5
S2	PCL/GEL-NHA (70%)/NC (30%)	62.5
S3	PCL/GEL-NHA (30%)/NC (70%)	62.5
S4	PCL/GEL-NHA (0%)/NC (100%)	62.5

to PCL solution and homogeneously mixed. Afterwards, the NHA and NC were blended with PCL-GEL at the prescribed concentrations listed in Table 1. The final ink was continually stirred in an open environment to modify the viscosity to an experimentally determined viscosity suited for 3D printing by evaporation of the solvent [25].

3D Printing of Nanocomposite Scaffolds

A 3D printer equipped with a single-screw microextruder (Abtin II; Abtin Teb Iran Company) was used for printing the prepared inks. The scaffold's geometry was designed using SolidWorks software (Solidworks version 2017; Dassault Syste`mes, France). Then, the final STL file was converted to G-code via Slic3r software. After transferring the ink into a 10 mL syringe, the porous 3D structures were printed layer by layer up to 20 layers via continuous ink extrusion through a nozzle of 22G (inner diameter = 410 µm). Finally, 3D scaffolds in dimensions of $20 \times 20 \times 6$ mm^3 with 500 µm strut spacing were printed at room temperature and speed of 3 mm/s.

Characterization of the Scaffolds

Determination of the Porosity

The porosity of the 3D printed scaffolds was detected using the liquid displacement method with hexane. Hexane was chosen as a transport fluid because it is able to pass through the scaffolds without causing the structure to inflate or shrink [26]. A scaffold that had previously been weighed was immersed for 5 min in a certain amount of hexane (V_1). The total volume of hexane and hexane-impregnated scaffold (V_2) was recorded. The scaffold was then removed from the hexane and the volume of the remaining hexane was measured (V_3). For each type of scaffold, the test was repeated three times. The following Eq. (1) was used to calculate the scaffold porosity (ε):

$$\varepsilon = \frac{V_1 - V_3}{V_2 - V_3} \times 100 \quad (1)$$

Morphology of the Scaffolds

The morphological analysis of the samples was performed using scanning electron microscopy (SEM, Philips XL30, Netherlands). Herein, the prepared scaffolds were gold plated and the SEM images were taken with an accelerating voltage of 20 kV. The size of the pore diameter was also quantified from randomly selected pores with Image J software (v.1.52a, National Institutes of Health, USA) through SEM images (taken at 50 × magnification) of the scaffolds.

Spectral Characterization of Scaffolds

FT/IR-6300 spectrometer spectra (JASCO, Japan) were performed in a wave number from 650 to 4000 cm^{-1} and 4 cm^{-1} resolution, in order to accomplish the chemical analysis of the 3D printed scaffolds. Moreover, the phase changes and purity of the scaffold materials were investigated using X-ray diffraction (XRD; Bruker, D8ADVANCE/Germany). The data was provided between $10° \leq 2\theta \leq 80°$

Mechanical Properties

A universal testing equipment (Hounsfield-H25KS-England) equipped with a 2.5 KN load cell was used to assess the stiffness of scaffolds in the dry state ($4.5 \times 4 \times 5$ mm^3). The axial load was applied at a rate of 5 mm/min up to a 50% strain level. The slope of the elastic portion of the scaffold stress–strain curve was used to compute the compressive modulus.

Contact Angle Measurement

The static contact measurement was performed using the sessile drop method utilizing CA-ES10 (Fars EOR. TechCo) at 25 °C. The contact angle was measured at regulated humidity, 10 s after a 5 µl water droplet was placed on the scaffold surface (n = 3).

Water Uptake Measurement

Water uptake investigations were conducted using dry-weighted scaffolds (W_d) submerged in PBS at 37 °C to assess the percentage of water uptake capability. Samples were taken out of solution at 1, 6, 12, 24, 48 h time points and their weight was recorded (W_w) after excess water removal [27]. The water uptake was computed according to the following Eq. (2) [28]:

$$\text{Water uptake}(\%) = \frac{W_w - W_d}{W_d} \times 100 \quad (2)$$

Bioactivity and Ion Release

The bioactivity of 3D printed scaffolds (n = 3 with equal geometry) was determined by immersing them in SBF at 37 °C for 7 and 28 days, according to the Kokubo protocol [29]. The solution was changed twice a week during the time of incubation, and the scaffolds were rinsed gently with pure water after removing from the SBF solution at each time point. Finally, the lyophilized scaffolds examined with SEM and the elemental distribution and composition of calcium, phosphorus, and silicate were also investigated via Energy-dispersive X-ray (EDX) analysis. The concentrations of calcium and phosphorus ions released from the scaffolds were measured by induced coupled plasma spectroscopy (ICP, Pekin Elmer-Optima 7300 DV). Herein, the PCL-GEL/NHA-NC scaffolds were cut into disks (n = 3) with 10 mm diameter, submerged in SBF and incubated at 37 °C. Then, the calcium and phosphorus ion release of 3D nanocomposite scaffolds were estimated on weeks 1 and 4.

Degradability Evaluation

In order to investigate the scaffolds' degradation behavior, they have been immersed in PBS (pH = 7.4) and kept for 3 months at 37 °C [30]. At one-week intervals, the pH changes were evaluated and then the scaffolds with previously known weight (W_0) were first removed from the solution, washed thoroughly with distilled water, dried in a vacuum oven at 45 °C overnight and weighted again (W_t). The degradation rate was defined according to the bellow Eq. (3):

$$\text{Degradationrate}(\%) = \frac{W_0 - W_t}{W_0} \times 100 \quad (3)$$

SEM images and FTIR analysis were employed to investigate the extent of scaffolds' degradation. EDX analysis was also conducted to evaluate the elemental distribution and composition of degraded scaffolds.

Cell Behavior on 3D Printed Scaffolds

Cell Culture and Seeding

The MG-63 cells are widely used as an osteoblastic model to investigate bone cell survival, attachment, and growth on the surfaces of scaffolds with load bearable properties [31]. MG-63 cells were obtained from Pasteur Institute, Tehran, Iran. The cells were cultivated in a cell culture flask containing DMEM, 10% FBS, and 1% penicillin/streptomycin and then kept at 37 °C in an incubator with 5% CO_2 until an appropriate level of confluency (80%) was attained. Prior to cell culture, the scaffolds were sterilized using gamma irradiation (25 kGy) for 20 min. Next, Trypsin/EDTA was used to harvest the cells from the culture flasks, which were then rinsed three times with PBS. A cell suspension (1×10^4 cells/well) was then seeded on the scaffolds placed inside a 24-well plate followed by transferring them to an incubator (37 °C, 5% CO_2).

Cell Viability

The MTT assay was conducted to determine the in vitro viability of adhered MG-63 cells on each scaffold after 1, 3, and 7 days, as previously described [32]. Cells at a density of 1×10^4 cells/well were seeded on 3D printed scaffolds and incubated at 37 °C with 5% CO_2. Monolayer culture of cells was also considered as a control group. At the end of each time point, the culture medium was carefully removed, washed with PBS and replaced with culture medium containing MTT (0.5 mg/mL). After 4 h of incubation, the MTT solution was discarded and 200 µL of DMSO was added to each sample (n = 3). The solutions were then transferred to a 96-well microplate and an ELISA reader (Bio-tek FLx800, USA) was used to detect the optical density (OD) at 570 nm wavelength. The cell viability (%) is normalized according to the following equation by the control group:

$$\text{Cells' viability}\ (\%) = \frac{\text{Sample wells' OD} - \text{BlankOD}}{\text{Control wells' OD} - \text{BlankOD}} \times 100 \quad (4)$$

SEM Images

SEM micrographs (Philips XL30, Netherlands) of cell seeded scaffolds were taken to assess the adherence and morphology of MG-63 cells. After one day of cell seeding on scaffolds, the cell culture medium was retrieved and fixed with 3% glutaraldehyde solution. Then, dehydration of the samples was performed with ethanol series of 50, 70, 90 and 100% for 10 min each one. Eventually, the samples were coated with a thin layer of gold and taken for SEM imaging.

DAPI Staining

The DAPI staining was used to evaluate cell density and spreading on nanocomposite scaffolds. Herein, a suspension of MG-63 cells (1×10^4 cells/well) was cultured on scaffolds and incubated for 7 days. After removal of the culture medium, the cell-seeded samples were washed with PBS, exposed to 4% paraformaldehyde for 20 min and placed in 1 µg/mL DAPI solution for 10 min. Finally, the images of MG-63 cell nuclei were captured with a fluorescent image analyzer (Nikon Eclipse Ti, Japan).

Statistical Analysis

The obtained results from laboratory experiments were presented in a form of mean ± standard deviation (SD). SPSS software V.23 was used to conduct statistical studies to clarify the differences between the groups through one-way analysis of variance (ANOVA) and Tukey's HSD post-hoc test. A value of $P < 0.05$ was considered as statistically significant.

Results and Discussion

Scaffold Porosity, Pore Size and Morphology

Scaffold porosity is essential for nutrient diffusion and metabolic waste products removal during cell proliferation. Moreover, porous scaffolds provides a 3D structure improving cell adhesion, migration and penetration [33, 34]. Figure 1a illustrates the measured porosity of 3D printed scaffolds. The S3 sample had the highest porosity among other samples, with 69.49 ± 1.19% porosity. The average porosity percentages gently decreased to 68.37 ± 1.80%, 61.98 ± 1.64% and 58.14 ± 1.08% for S1, S2 and S4 samples, respectively. In comparison to the other groups, the S2 and

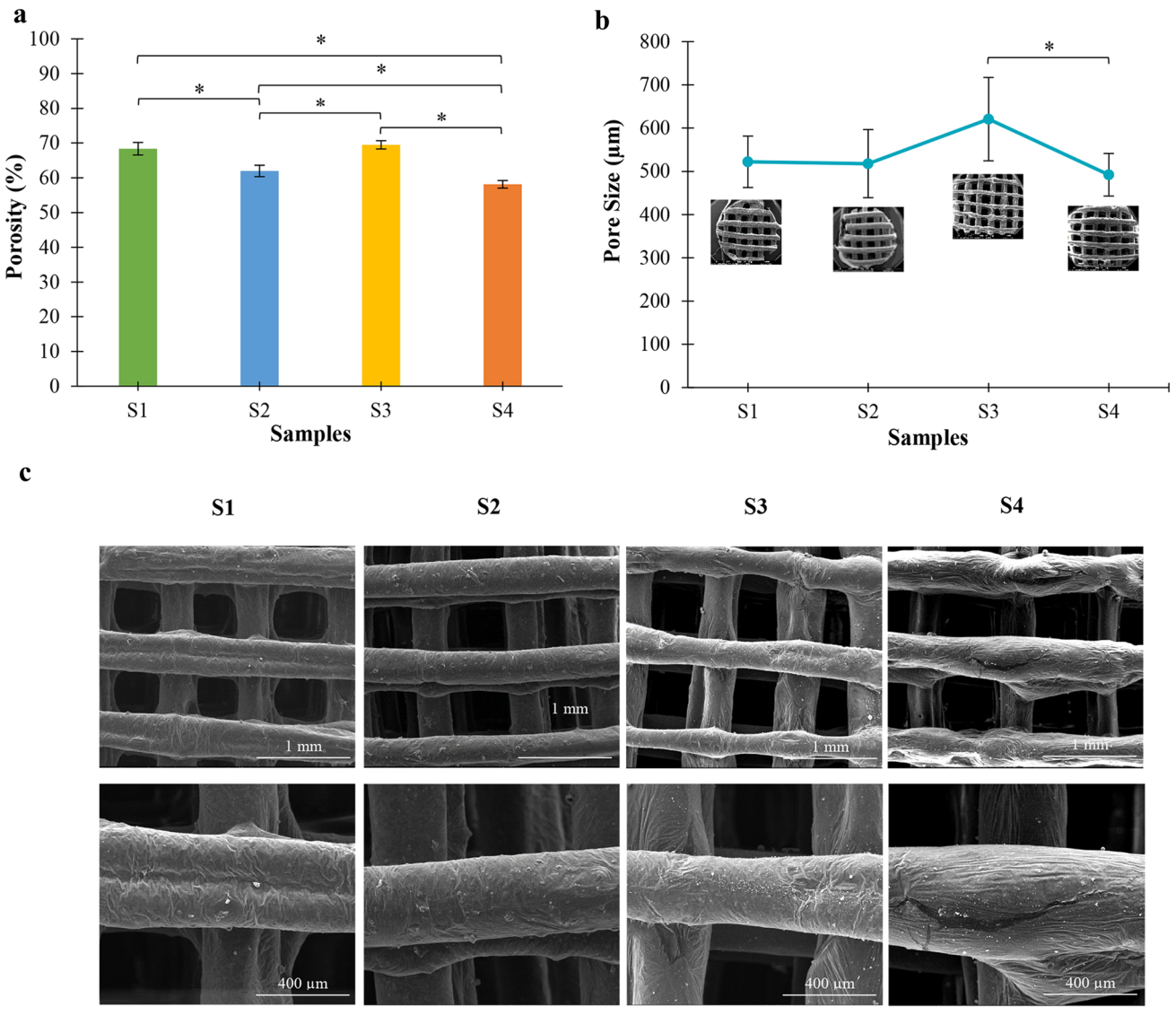

Fig. 1 **a** Porosity percentage, **b** average pore size and **c** SEM images of the 3D printed scaffolds at different scale bars with various amount of NHA and NC (values are mean ± SD, $n = 3$, *$P < 0.05$). Significant differences between the samples are shown by (*$P < 0.05$)

S4 samples exhibited the lowest porosity values. Figure 1b, c illustrate the morphology and mean pore sizes of the printed composite scaffolds. As can be seen in SEM images, all of the printed samples are structures with interconnected and rectangular shaped pores. Moreover, NHA and NC particles distribution can be seen throughout the scaffold surfaces and a high level of filament shape stability and accuracy was apparent in all printed scaffolds. The highest average porosity size was seen in sample S3; although it was only significant with the S4 sample ($P < 0.05$), which is the result of decreasing filament diameter due to the enhanced surface tension associated with the use of specific concentrations of NHA and NC in S3 sample.

Kazemi et al. reported that addition of NHA to the scaffolds increases the stability of the filaments and decreases the ink spreading, leading broadening pore size and porosity percentages [35]. Furthermore, it has been demonstrated that composite networks are more likely to form porous structures when NC is involved [36]. According to previous findings, the required porosity and pore size for bone scaffolds is in the range of 60–90% and 100–600 µm respectively which is suitable for angiogenesis, cell migration, and bone ingrowth [10, 37, 38]. Thus, it can be concluded that NHA

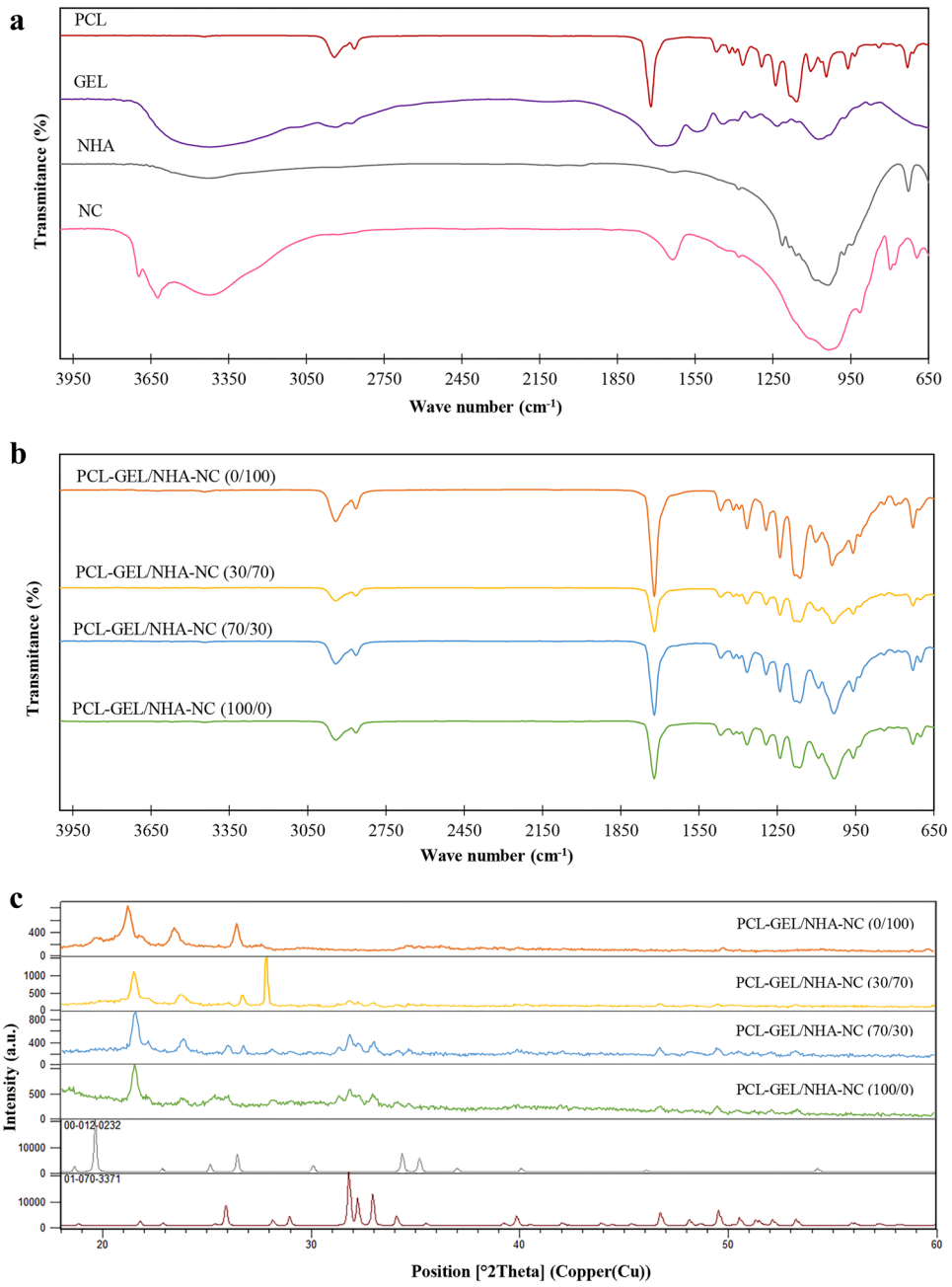

Fig. 2 FTIR spectra of **a** pure PCL, GEL, NHA, and NC and **b** PCL-GEL/NHA-NC (100/0, 70/30, 30/70, 0/100) scaffolds with **c** their XRD pattern

incorporation was more successful in improving the printability of the nanocomposite scaffolds.

Spectroscopic Characterizations of the Composite Scaffolds

FTIR Results

By employing FTIR, the functional groups of pure PCL, GEL, NHA, and NC as well as their composites were evaluated and the obtained results are presented in Fig. 2a, b. The FTIR spectrum of PCL demonstrated that 2865 and 2941 cm^{-1} peaks relate to symmetric and asymmetric CH_2 group stretching, respectively and the sharp peak at 1721 cm^{-1} belonged to C = O stretching. The band at 1159 cm^{-1} is ascribed to symmetric stretching of the C–O–C group, while the asymmetric C–O–C stretching appeared at 1240 and 1294 cm^{-1} [2]. The GEL spectrum showed major peaks at 1542, 1660, 2935, and 3421 cm^{-1} which are attributed to the vibrations of N–H bending, C = O stretching, alkenyl C–H stretching, and N–H stretching, respectively. Also other peaks were observed at 1442 cm^{-1} (CH_2), 1233 cm^{-1} (NH), 1076 cm^{-1} (C-O stretching) [39]. As can be seen in FTIR spectrum of NHA, the NHA spectrum contains the characteristic peaks at 3428 cm^{-1} (OH stretching vibrations), 1630 cm^{-1} (OH group bending), 1405 cm^{-1} (carbonate group vibration), peaks at 1084 cm^{-1} (asymmetric stretching of PO_4^{3-}), 1036 cm^{-1} (asymmetric stretching of PO_4^{3-}), and 976 cm^{-1} (symmetric stretching of PO_4^{3-}) [40]. The NC spectrum showed prominent peaks at 797 cm^{-1} due to Si–O-Al vibration, 1033 cm^{-1} due to Si–O-Si stretching, 1637 and 3425 cm^{-1} due to O–H stretching of absorbed H_2O in NC, and 3623 cm^{-1} was attributed to the stretching mode of the Si–OH and Al–OH in the silicate layers of NC [41]. The composite scaffolds almost showed a similar spectra and strong PCL peaks can be clearly seen in all of the obtained spectra. As can be seen, the peaks found in the range of 727 cm^{-1} (symmetric stretching of PO_4^{3-}) [42] and 795 cm^{-1} became stronger with increasing NHA and NC concentrations, respectively indicating the existence of HA and NC in the composite scaffolds. Additionally, the peak at 1060 cm^{-1} (C–C vibration) [43] related to PCL was disappeared in composite scaffolds and changed into a broad peak, then shifted to the 1029 cm^{-1}, which may be associated with the strong NHA peak at this region. According to earlier research, the first indication of NHA in an FTIR spectrum is the presence of a broad peak between 1000 and 1100 cm^{-1} [44, 45]. However, it seems that with the increase of NC concentration, the shifted peak had the least change due to Si–O-Si stretching vibration peak in NC. Identifying GEL peaks in the spectrum of the scaffolds might be challenging due to its low concentration in the composite scaffolds and overlapping its mild peaks with other material peaks. However, other studies have proven that adding GEL to PCL shifts the FTIR spectrum peaks to lower wavelengths [2, 46] which is consistent with this study in term of shifting a PCL peek at 1104 cm^{-1} (O–C vibration) [47] to shorter wavelengths. It is evident from the composite scaffolds FTIR pattern that the characteristic bands of PCL, GEL, NHA, and NC are distinguished.

XRD Results

Figure 2b presents the XRD patterns of the S1 to S4 samples. As can be seen, the XRD pattern of the 3D printed scaffolds exhibits two distinct peaks at $2\theta = 21.5°$ and $2\theta = 23.8°$ that are indicative of the crystal structure of PCL [48]. Previous studies have also indicated that incorporation of GEL to PCL simply lowers the PCL peaks intensity due to the amorphous nature of GEL. Reducing PCL peaks intensity results in decreased crystallinity rate of the nanocomposite scaffolds, confirming PCL-GEL molecule interactions [48, 49]. The XRD results of the NC contained scaffolds demonstrated that the polymer chain was introduced into the NC interlayer domain since the typical peak of NC was found near at $2\theta = 19.8°$ and 26.45° which are matched with JCPDS Card No 00–012-0232.[50, 51]. The crystalline nature of the NHA powder was evident by the presence of peaks approximately at $2\theta = 26°$, 31.35°,32.25°, 33.05° and 49.55° (JCPDS Card No 01–070-3371) [49] which could be seen after addition of NHA to the prepared scaffolds. These findings imply that the molecules of the PCL-GEL/NHA-NC scaffold may interact with each other.

Mechanical Characterization

For sufficient cellular and tissue support, utilized scaffolds for healing bone defects should have appropriate mechanical properties [52]. The compressive strength and stiffness of the composite scaffolds were investigated in this study. Figure 3a depicts the stress–strain curves of the fabricated scaffolds at a strain level of 60%. All of the printed scaffolds exhibited similar stress–strain behavior, which was consistent with the normal response of polymeric porous scaffolds, and as the NC amount increased, compressive strength also enhanced significantly ($P < 0.05$). However, the highest stiffness value belonged to the S3 sample (35.21 ± 1.31 MPa) and conversely, the sample with NHA/NC (70/30) possessed the lowest deformation resistance (11.18 ± 2.13 MPa) compared to the other scaffolds. The PCL-GEL/NHA sample also exhibited more rigidity than the PCL-GEL/NC sample, although the difference was not statistically significant ($P > 0.05$). These outcomes may be correlated with the earlier determined porosity percentage of 3D printed scaffolds. Moreover, due to NHA's greater brittleness compared

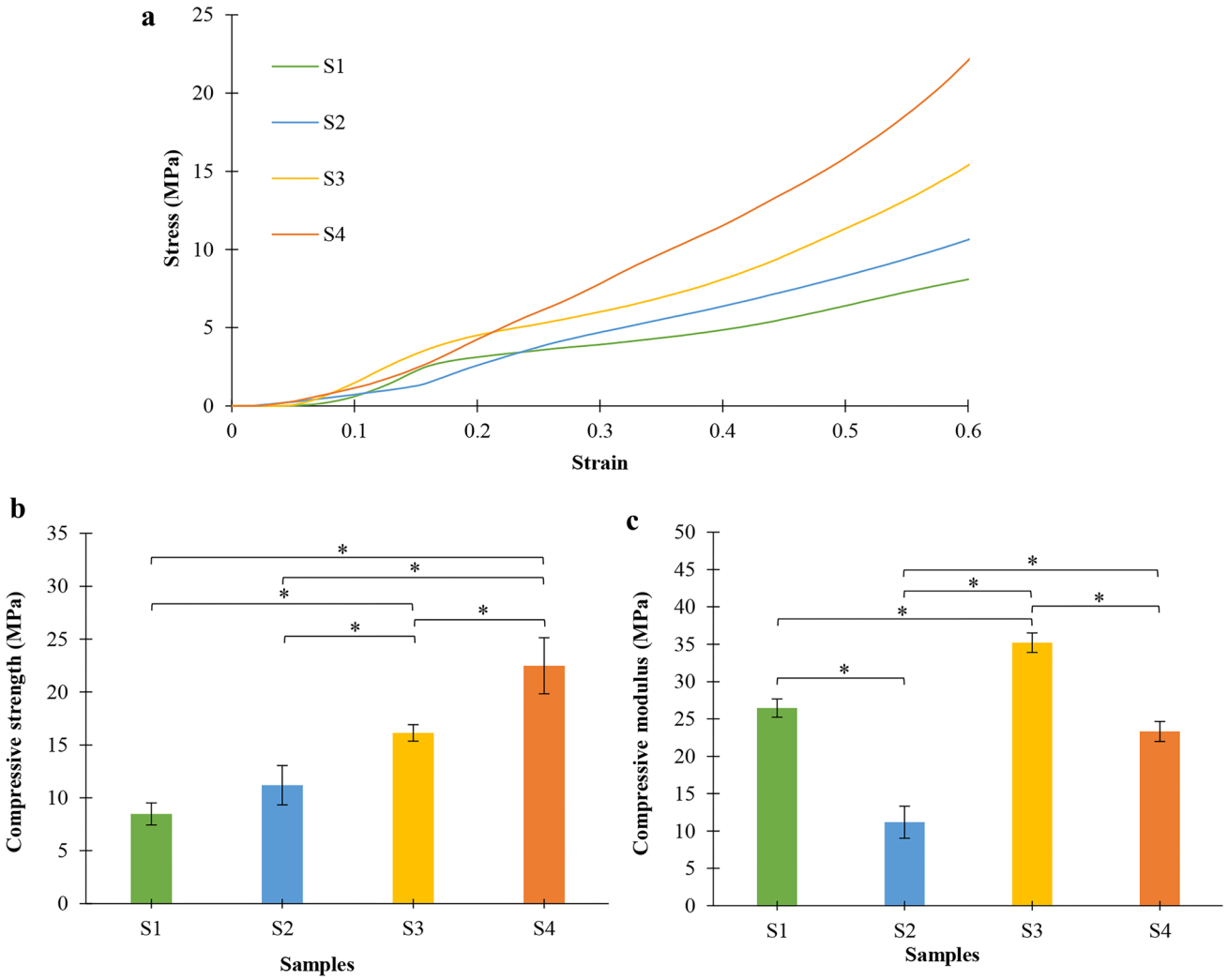

Fig. 3 Mechanical evaluation of the nanocomposite scaffolds. **a** The scaffolds' stress–strain curves under uniaxial compression loading. **b** The compressive strength and **c** Compressive moduli of the 3D printed scaffolds (values are mean ± SD, $n = 3$, *P < 0.05). Significant differences between the samples are shown by (*P < 0.05)

to PCL-GEL scaffolds, it may enhance the brittleness of PCL-GEL/NHA samples, which reduces their compressive strength. In addition, accumulation of NHA crystals may occur in composite scaffolds, resulting in a poor interaction between the NHA and PCL-GEL scaffolds [53]. Nevertheless, inorganic fillers such as layered nanosheets of NC can reinforce scaffolds through uniform distribution and interaction between nanosilicates and polymer matrix [54]. Comparing the compressive strength and stiffness of human bone and the 3D printed scaffolds reveals that the composite scaffolds are still weaker than cortical bone (strength of 100–230 MPa and stiffness of 7–30 GPa [55, 56], but it is comparable with the cancellous bone (strength of 2–12 MPa and stiffness of 0.01–3 GPa [56, 57]).

Wettability of the Scaffolds

A crucial property for bone scaffolds is wettability which determines appropriate cell attachment and accelerates oxygen and nutrients delivery [58]. The water contact angle test of all types of 3D printed scaffolds was performed and shown in Fig. 4a. The S4 sample exhibited the lowest contact angle (52.45 ± 1.028°) compared to other three samples. Earlier studies reported that PCL has a contact angle greater than 100°, indicating its hydrophobic nature [32, 59], and adding GEL reduces the PCL contact angle to the 70–80° range due to its hydrophilic chemical groups (amide group) [60, 61]. By adding NHA to PCL-GEL scaffolds, the contact angle value has reached to 64.216 ± 1.509° and incorporation of NC with 30 wt% and 70 wt% concentration has significantly reduced the

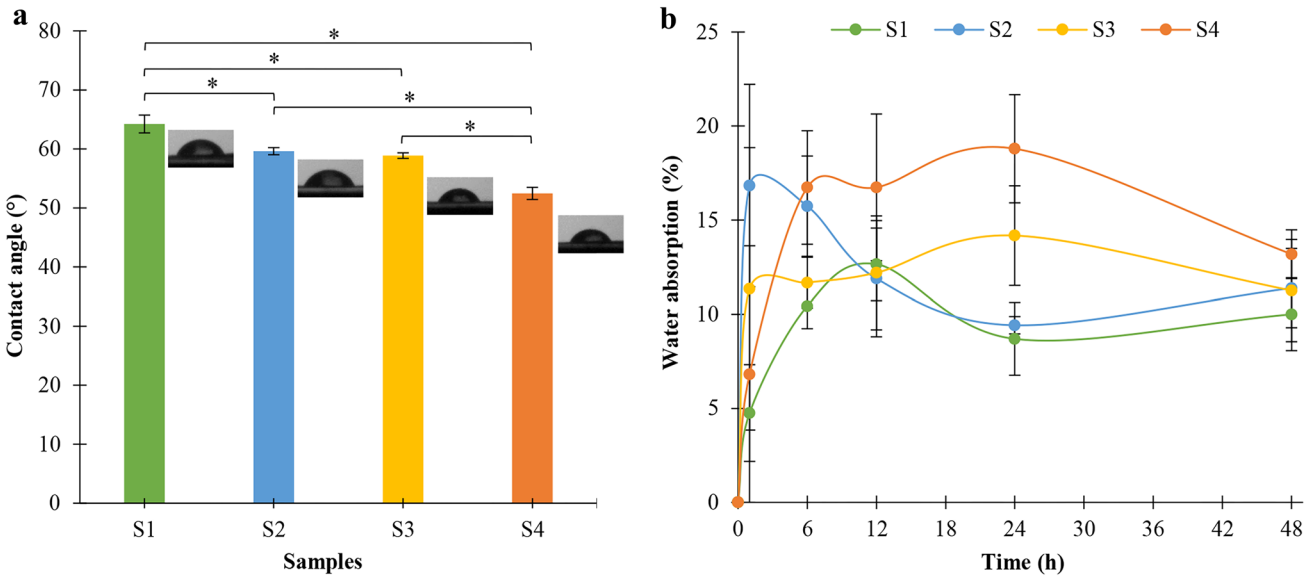

Fig. 4 **a** Water contact angle comparison for samples S1 to S4 based on NHA and NC concentrations. **b** Water absorption of S1 to S4 after 1, 6, 12, 24, and 48 h incubation in PBS (values are mean ± SD, $n = 3$, *P < 0.05). Significant differences between the samples are shown by (*P < 0.05)

average contact angle of PCL-GEL/NHA scaffolds to 59.609 ± 0.603° and 58.859 ± 0.472°, respectively (P < 0.05). In this regard, previous investigations also reported that the wettability of PCL scaffolds increased after adding NC and NHA to PCL due to the hydrophilic property of NC and NHA [62, 63]. Moreover, Rajzer et al. proved adding NHA to scaffolds enhances surface roughness due to the presence of additional crystallites on the surface of scaffolds, which raises the contact angle [64]. The general conclusion of this section was that high amounts of NC considerably improved the PCL-GEL scaffolds wettability and brought the highest level of hydrophilicity compared to other groups.

Water Uptake of the Scaffolds

Figure 4b shows the water uptake capability of fabricated scaffolds at various time intervals. The S1 sample without NC incorporation exhibited less water uptake rate. However, as the concentration of NC increased in the scaffolds, the initial water uptake rate reduced but its amount enhanced over time. Furthermore, the PCL-GEL/NC sample showed the significantly highest value of hydration equilibrium after 24 h compared to the S2 and S1 samples (P < 0.05), followed by a slower water release compared to the PCL-GEL/NHA sample. As previously stated, PCL is reluctant to absorb water due to its hydrophobic nature, and several studies have been conducted to improve the water uptake capacity of this polymer, including the combination of GEL with PCL [65–67]. In this study, NC participation had the most positive effect on increasing water uptake capability of PCL-GEL scaffolds due to its hydrophilic property, allowing inorganic cations in the interlayer to hydrate [68]. The potential of scaffolds to absorb water is very crucial since it regulates the exchange of nutrients and metabolites among cells [69]. Despite the fact that it has been mentioned in other studies that adding NHA reduces gelatin's hydrophilicity by binding calcium (Ca) and phosphate to hydrophilic carboxyl (COOH) or amine (NH_2) groups, it prevents the penetration of water into the scaffold due to the temporary barrier created by NHA, and subsequently reduces the water uptake of the nanocomposite scaffolds [58]. Moreover, due to the barrier effect of NC nanosheets, water molecules are inhibited from interacting with the macromolecules of polymers, resulting in low water content levels [53]. Thus, utilizing a suitable amount of NHA and NC in the PCL-GEL scaffold matrix is a potential method for controlling water uptake.

Bioactivity and Ion Release Behavior

Bioactivity

The ability of a biomaterial to bond with bone is often determined by testing the formation of NHA on the surface of the sample. According to Hench Theory, the formation of NHA starts with dissolution. In other words, this process begins with dissolution and release of calcium ions on the surface of the sample towards the solution [61, 70]. Ion release and dissolution is defined in terms of the scaffold degradability. In this study, four samples have the same amounts of

PCL and GEL. Many studies have confirmed the degradability and the bioactivity of PCL [61, 70]. PCL is a bioactive synthetic polymer. Due to the presence of ester and water-sensitive groups, it will undergo hydrolysis process after exposure to biological environments [61, 71]. The formation of carboxyl groups on the hydrolyzed PCL surface leads to the release of positively charged hydrogen ions (H^+) from COOH towards the SBF environment. The release of H^+ cation will decrease the pH of the environment and increase the tendency to dissolve the scaffold surface [72]. The release of positively charged ion (H^+) followed by the formation of COO^- anion on the surface leads to the electrostatic attraction between PCL and calcium cations (Ca^{2+}) present in SBF [71]. The presence of GEL as a peptide biopolymer is one of the effective factors in creating nucleation sites in the formation of Ca-P deposits [61]. GEL easily reacts with aqueous environment and leads to the formation of positively charged NH_3^+ and negatively charged COO^- ions respectively due to its amine (NH_2) and carboxyl groups [61, 71]. Electrostatic attraction and repulsion between the positive and negative ions of the SBF environment and the surface of the scaffold leads to the formation of calcium-phosphate deposits [61, 70]. The presence of NHA in the structure of the scaffolds is another effective factor in increasing the dissolution and release of ions from the scaffold towards the solution. The presence of NHA will also leads to the creation of nucleation sites [72]. Studies have reported that the presence of NC has a direct effect on the creation of nucleation sites [73]. The presence of SiO_4^{4-} negatively charged ion caused by the presence of clay is effective in creating negatively charged cyanol (Si–OH) layers as a silicate material. These negatively charged layers lead to the electrostatic attraction

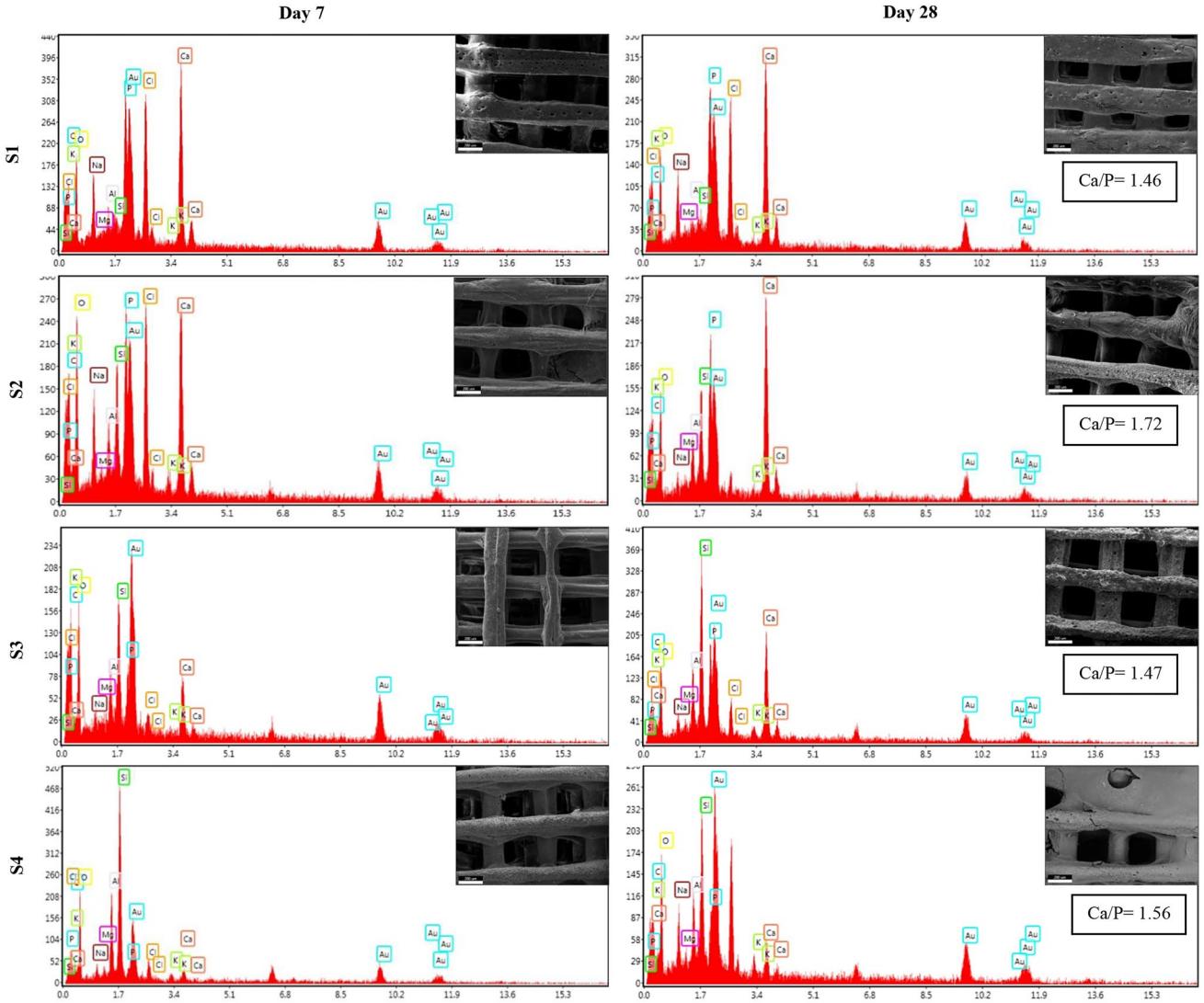

Fig. 5 Elemental analysis of S1 to S4 samples with SEM images after 7 and 28 days immersed in SBF to confirm the existence of Ca and P on the samples' surface (scale bars = 200 µm)

of Mg^{2+} and Ca^{2+} cations on the surface of the scaffold. According to the data obtained from EDS analysis during 7 days of immersion in SBF (Fig. 5), increasing the amount of NHA from 0 to 1wt. % has led to the increase of calcium and phosphorus on the surface of the scaffold. This could indicate the effect of NHA in increasing deposition. The presence of calcium and phosphorus cations in the synthesized NHA in the scaffold is also effective in increasing the amount of these two elements. In ion exchanges between the surface of the scaffold and the SBF environment, there is a competition for deposition and interaction with the surface of the scaffold between the two Ca^{2+} and Mg^{2+} cations [35]. It is necessary to reduce the deposits containing MgO and Mg_2SiO_4 in order to form crystalline deposits of NHA (calcium-phosphate) [35]. According to the elemental data, it can be stated that the amount of Mg on the surface of the S1 sample has decreased compared to other scaffolds. This can indicate the dominance of Ca^{2+} over Mg^{2+} in interaction with the surface of the scaffold. The formation of MgO and Mg_2SiO_4 phases has also decreased. The amount of Mg in the NHA-free scaffold has increased compared to other scaffolds and reached 0.22 wt.%. These results demonstrate the effect of NHA compounds in the formation of calcium-phosphate deposits. On the 28th day of immersion, the S1 and S2 scaffolds has more calcium and phosphorus compared to the other scaffolds. In addition, EDX analysis

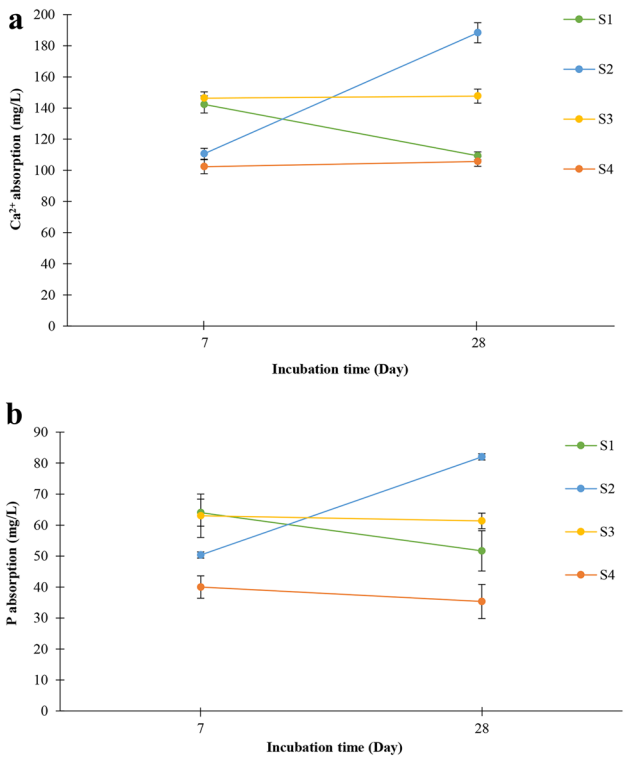

Fig. 6 **a** Ca^{2+} absorption (mg/L) and **b** P absorption (mg/L) of S1 to S4 samples in SBF during 1 and 4 weeks

indicated that the Ca/P ratios of the samples were consistent with nonstoichiometric biological apatite, which was found to be approximately around 1.67 after immersion in SBF for a period of four weeks, which is in line with the results obtained from a previous study [10].

Ion Release

According to the ICP results (Fig. 6), the amount of calcium and phosphorus in the SBF solution related to the S1 scaffold is higher than other scaffolds. This can indicate the greater dissolution of NHA in the scaffold, the decrease in pH of the environment and the release of calcium and phosphate ions from the scaffold toward the solution, which has increased the concentration level of these two elements in the solution. The surface roughness caused by the presence of NC is also one of the other effective factors in creating nucleation sites [73]. Based on the ICP results, the S4 sample shows lower amounts of calcium and phosphorus compared to the other scaffolds, during 28 days in solution. The decreasing trend of calcium and phosphorus in clay-free scaffold solution during 28 days indicates the increase of the tendency of these two elements to interact with the surface. In the S2 sample, the amount of calcium and phosphorus in the solution has increased during 28 days. This can indicate the release of anions and cations from the surface of the sample toward the solution, which is one of the requirements of ion exchange to create calcium-phosphate deposits [61, 70]. In other words, after placing the S2 sample in SBF solution, HPO_4^{2-} anion and Mg^{2+} cation release from the surface and increase the amount of phosphorus after dissolving in the solution. The amount of calcium in the solution has increased due to the decrease in the amount of phosphate ions and calcium cation deposits on the surface of the scaffold. According to the data obtained from the elemental analysis on the 7th and 28th day, the S2 sample has performed better than the S3 sample in terms of the creation of nucleation sites and the formation of calcium-phosphate deposits. This shows the great influence of NHA in the formation of minerals. The increase of calcium-phosphate deposits on all the scaffolds during 28 days indicates the bioactivity of the scaffolds. GEL as a polypeptide and PCL as a polyester undergo hydrolysis process after being placed in a simulated body environment at 7.4 pH and 37 °C and create positively charged NH_3^+ and COO^- ions respectively [61, 70, 71]. The presence of COO^- along with the formation of Si–OH negatively charged cyanol layer participates in attraction of Ca^{2+} and Mg^{2+} cations. The increase of calcium deposits compared to magnesium is critically important in bioactivity. The attraction of cations leads to the creation of nucleation sites on the surface of the scaffolds. Providing

the substrate chemically (the presence of cations) and morphologically (roughness of the surface due to the presence of NC) as well as the bioactive nature of NHA and NC in the structure of the scaffolds, are effective factors in creating bioactive properties. After providing a cationic substrate caused by calcium deposits and NH^{3+} present in GEL, HPO_4^{2-} and SiO_4^{4-} anions (caused by silicate layers present in clay) interact with surface cations through electrostatic attraction of dissimilar charges. The attraction between calcium and NH^{3+} cations and HPO_4^{2-}anions lowers the energy barrier for the formation of Ca-P (calcium-phosphate) crystal deposits and facilitate the formation of them [35].

Biodegradability

In bone tissue engineering, the scaffold's rate of degradation must be adjusted to maintain the required structural support until the recently formed bone is strong enough to take over the supporting role. Without meeting this requirement, the fabricated scaffold may fracture when subjected to mechanical force before bone healing has taken place [74]. The current investigation evaluated the nanocomposite scaffolds' degrading behavior over a 12-week period of soaking in PBS (pH 7.4). The findings were displayed in Fig. 7, which included plots showing weight and pH changes during the soaking period as well as FTIR analysis and SEM images of the degraded samples after 12 weeks.

During the process of degradation, scaffolds will experience cycles of water absorption and desorption, which is why the weight loss rate of the samples is shown as a fluctuating graph curve (Fig. 7a). The hydrolysis process takes place in three steps which are absorption, interaction and release [75]. Hydrophilic amine groups in GEL, PCL ester groups, silicate in clay, and phosphate and calcium ions in the NHA structure are all components that contribute to the scaffolds' ability to absorb water. Water molecules act as a softener for PCL-GEL polymer chains and will increase the mobility and the volume of the chains and separate their connections [75]. Moreover, Fig. 7a displayed the degradation rate for all scaffolds starting at eighth week. The inclusion of NC in the S4 and S3 samples, respectively, has increased hydrophilicity compared to other scaffolds, and Fig. 7a displayed a higher weight loss until the twelfth week. The

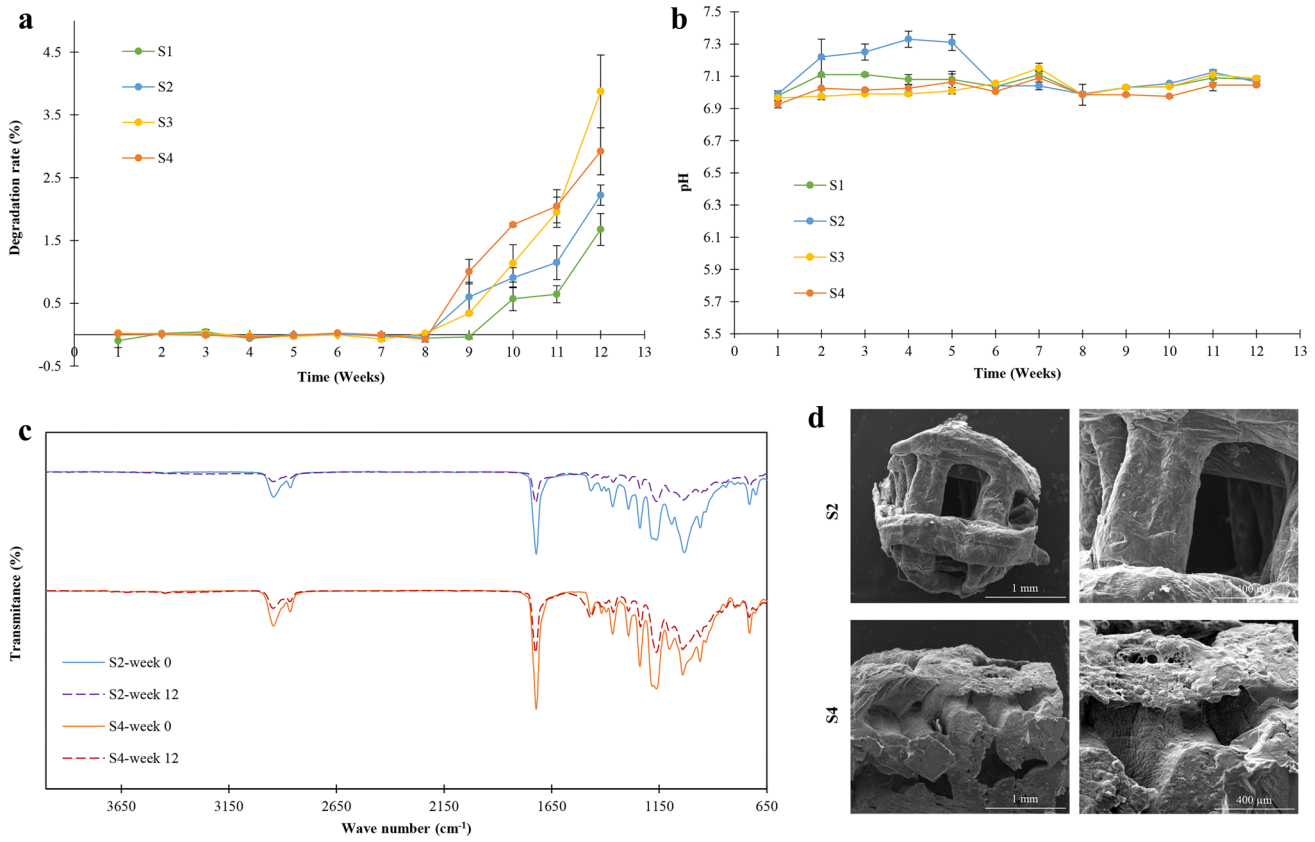

Fig. 7 **a** Degradation rate of the S1 to S4 nanocomposite scaffolds during 3 months. **b** The pH changes after soaking the S1 to S4 samples in PBS solution during 3 months. **c** FTIR spectra of S2 and S4 samples at 0 and 12 weeks' time point soaked in PBS. **d** SEM images of S2 and S4 samples after 3 months degradation in PBS at different scale bars (values are mean ± SD, $n = 3$, *P < 0.05)

scaffolds' tendency to absorb water increases as they become more hydrophilic. The hydrophilicity findings indicated that S1 sample is less hydrophilic than other scaffolds while S4 and S3 scaffolds, respectively, are more hydrophilic due to the presence of oxygen groups in SiO_4^{4-}. Due to the presence of clay, SiO_4^{4-} is ready for ionic and polar interactions with NHA cations and other positively charged polar groups of the scaffold. The weight loss percentage over 12 weeks revealed that S1 and S2 samples have the degradation rate of $1.67 \pm 0.25\%$ and $2.22 \pm 0.16\%$ respectively, and the highest weight loss percentage of $3.87 \pm 0.57\%$ belongs to S3 sample. The S4 scaffold had a weight loss percentage of $2.92 \pm 0.37\%$ and there was a significant difference between the weight loss percentage of S1 and S2 scaffolds with S3 and S4 samples ($P < 0.05$). The increased percentage of weight loss in the S3 sample demonstrated the impact of the structure's increased hydrophilic group content. The rate of weight loss has increased from 2.22 to 3.87% as a result of increasing the amount of NC from 30 to 70 wt%. The quantity of free polar groups available to interact with water molecules has grown due to the presence of NC with increasing the hydrophilicity. Generally, the percentage of weight loss rose with an increase in the amount of NC in the structure. NC with negatively charged groups along with other polar groups such as carbonyl (C = O) from PCL, NH_2 and COOH from GEL, and HPO_4^{2-} and Ca cations from NHA can enhance the tendency of chemical interactions and hydrolysis. According to pH changes (Fig. 7b), ions have been released from all of the scaffolds and cations have been dissolved into the PBS solution, raising pH up until the fourth week. GEL's amino acid structure contains COOH, which releases H^+ to lower pH levels in the physiological aqueous environment [61]. Additionally, water and acid are produced by the reaction of the ester group of PCL with the aqueous medium, which also lowers the pH. The decrease in pH will improve the solubility of NHA [61, 72, 75], which causes the release of calcium cations and HPO_4^{2-} from the scaffold into the solution. All scaffolds exhibited pH fluctuations over the period of 12 weeks, which may be caused by ion exchanges and electrostatic interactions between charged groups of scaffolds [72, 73]. Throughout the degradation process, each scaffold maintained the pH within the physiological range, and the solution recovered its buffer condition. It is evident from the FTIR spectra (Fig. 7c) of the S4 and S2 samples that after 12 weeks, the height of the characteristic PCL peaks has diminished, indicating that the scaffolds' inclusion of NC and NHA nanoparticles has improved the degradation of PCL. The SEM images (Fig. 7d) of the S2 and S4 samples clearly depicted eroded surfaces after 12 weeks of immersion in PBS. The S4 sample had more obvious signs of degradation than the S2 sample. The S4 scaffold surfaces had more visible cracks and holes, which revealed a rougher matrix due to the hydrolytic degradation. Previous research has demonstrated that gelatin's considerable biodegradability caused it to accelerate the deterioration of the PCL scaffold when it was added [76, 77]. Furthermore, it has been demonstrated that the inclusion of NHA nanoparticles accelerate the degradation rate of PCL scaffolds. By adding NHA, water and solvent are able to pass through the interface between NHA and PCL, making it more convenient for water to infiltrate the PCL matrix [78]. Adding NC also accelerates PCL scaffold degradation, which might be brought on by PCL-NC composite's reduced hydrophobicity. The inclusion of nanoclay might make it easier for water to adsorb, preparing PCL chains for hydrolysis [71].

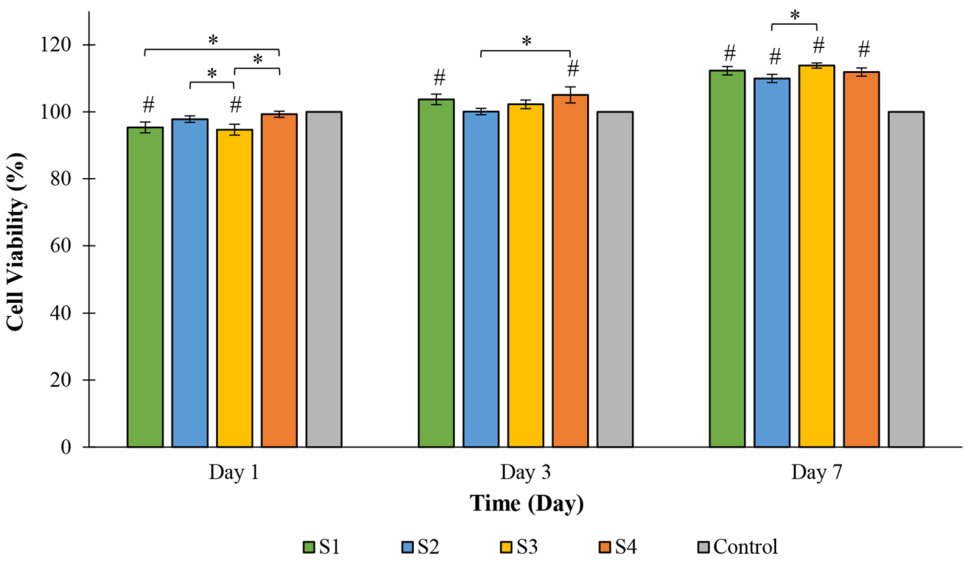

Fig. 8 The viability of MG-63 cells on the 3D printed scaffolds during 1, 3, and 7 days (Values are mean ± SD, $n = 3$, *$P < 0.05$). Significant differences between the samples are shown by (*$P < 0.05$). The number sign ($^{\#}P < 0.05$) denotes a difference that is statistically significant when compared to the control group

Cell Compatibility

One of the most fundamental challenges in tissue engineering is cell compatibility of biomaterials [79]. As a result, the MTT test was used to determine the biocompatibility of each scaffold. The cell viability of each 3D printed sample after 1, 3, and 7 days of incubation is illustrated in Fig. 8. After the third day, all scaffolds showed a cell viability rate of at least 100%, indicating the scaffolds' high biocompatibility [80]. As can be seen, the sample without NHA incorporation had the highest cell viability rate ($99.27 \pm 0.91\%$) on the first and third days. In addition, the S1 and S3 samples illustrated significantly lower cell viability than the control group and the S4 sample on the first day ($P < 0.05$). After one week, all scaffolds showed a significant increase in cell viability rate compared to the control group ($P < 0.05$) and the highest MG-63 viability was attributed to the scaffolds with high NC concentrations (S3 and S4). Our findings are consistent with prior studies using NC, which determined that this mineral can improve cell compatibility of scaffolds and allow them to proliferate and differentiate in its presence without any side effects [81–84]. It's worth noting that NHA is also mentioned as a very effective nanoparticle in cell proliferation when added to PCL-GEL scaffolds [2, 46], and the employment of this nanoparticle in combination with NC has formed a suitable structure for better cell proliferation.

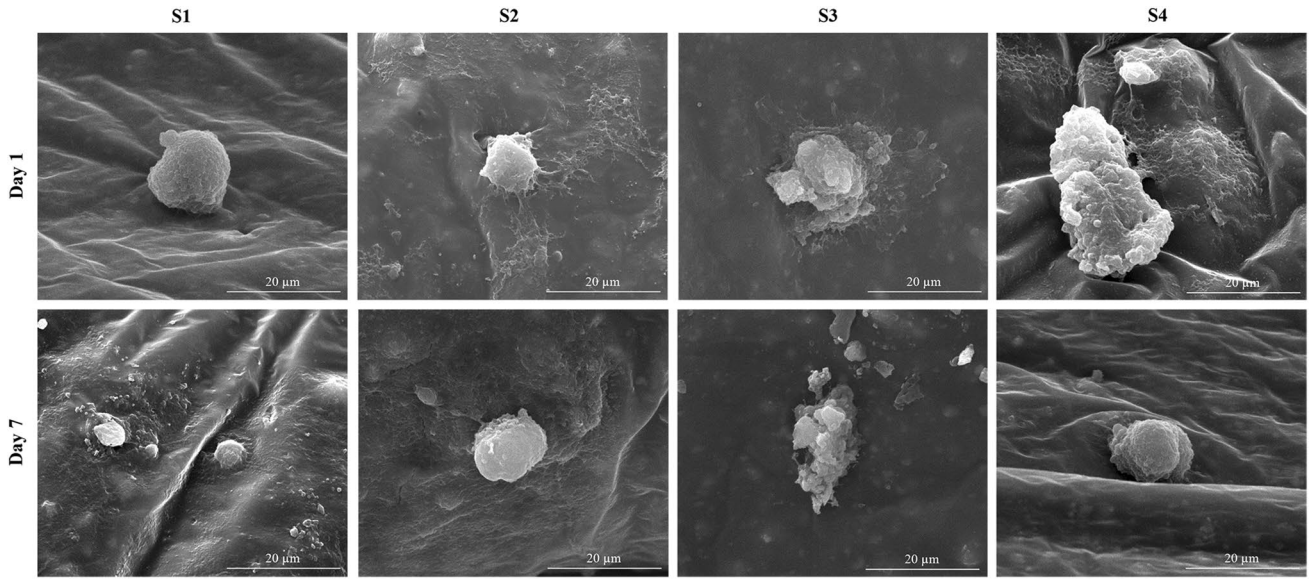

Fig. 9 SEM images of the cell-seeded scaffolds after days 1 and 7, demonstrating the MG-63 cells morphology and adherence at various scale bars

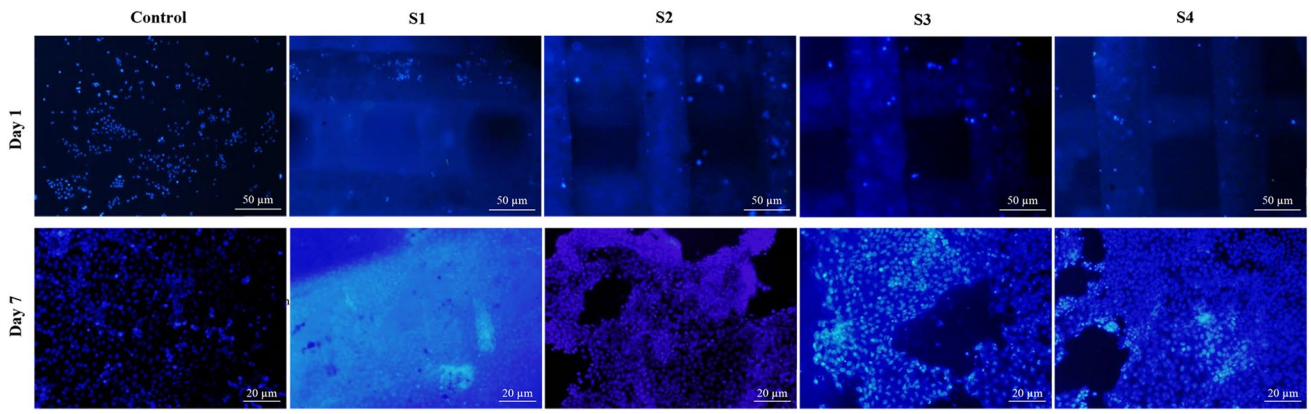

Fig. 10 DAPI stained MG-63 cells on the S1 to S4 scaffolds on days 1 and 7 were observed in the obtained confocal images at different scale bars

Cell Attachment

The MG-63 cells' adherence to the composite scaffolds was evaluated by SEM images after 1 and 7 days post-seeding in Fig. 9. The results clearly demonstrated that the cultured cells are well adhered on the scaffolds and exhibited a spread-out morphology and structures that extended to the scaffolds in the form of pseudopodia. Additionally, it seemed that cells attached to the scaffolds more as the NC concentration was increased. DAPI staining images of cultured MG-63 cells on 3D printed scaffolds after 1 and 7 days are illustrated in Fig. 10. DAPI is a fluorescent nucleic acid dye which binds to DNA very tightly, and it is commonly used in chromosome staining [85]. The arrangement of cell nuclei was apparent on each composite scaffolds after DAPI staining. According to the results, each scaffold had a considerable rise in cell number compared to the control group after one week, which is also consistent with the MTT results. Moreover, the cells' uniform distribution and high density on the scaffolds can clearly be seen at day 7. Previous studies have indicated that NHA enhances the surface area and roughness of the scaffolds' surfaces, which improves cell adherence to scaffolds in addition to its important function in the primary adsorption of bone adhesive proteins [46, 86]. Another study has revealed that increasing NC has a beneficial impact on cell adhesion and proliferation [87]. The montmorillonite NC, same as NHA, has the ability to provide multiple active sites for the adsorption of adhesive proteins such as vitronectin or fibronectin to facilitate the diffusion of bone cell actin filaments on the fabricated scaffolds [73, 88]. Furthermore, it increases the number of bone cells that attach to the scaffolds by making their surfaces rough [54]. The enhanced concentration of divalent ions (Ca^{2+} or Mg^{2+}) along NC surfaces may also be responsible for better cell adhesion, since the divalent cations facilitate cell-ECM interactions through transmembrane receptors called integrins [73, 89].

Conclusion

In the present investigation, PCL-GEL composite scaffolds containing various concentrations of NHA and NC were fabricated using 3D printing technology, and the physicochemical and cellular properties were assessed in *vitro*. The SEM micro-images of the fabricated nanocomposite scaffolds revealed interconnected pores with acceptable size and a suitable porosity percentage. The hydrophilicity of the scaffolds was effectively improved as the concentration of the NC enhanced. The 3D printed PCL-GEL/NHA scaffolds with the addition of NC showed potential for use in bone tissue engineering as well, according to the appropriate mechanical, bioactivity and biodegradability properties. Due to the bioactive nature of these compounds, in *vitro* culturing of MG-63 cells revealed higher proliferation and viability on the NHA and NC contained scaffolds. Taking together, it suggests that the PCL-GEL/NHA-NC scaffold might be able to regenerate the bone defects, which obviously further studies are required to assess the clinical validity.

Acknowledgements The authors gratefully acknowledge the scientific support for this work by the University of Central Tehran Branch, Isfahan and Isfahan University of Medical Sciences (IUMS).

Author Contributions Saba Nazari: Conceptualization, methodology, validation, formal analysis, writing Original draftDr. Mohammed Rafienia and Dr.Mitra Naeimi: Conceptualization, methodology, validation, writing review, and editingDr. Majid Monajjemi: Writing review and editingDr.Seyed Ali Poursamar: methodology, validation, formal analysis

Funding This research did not receive any specific grant from funding agencies in the public, commercial, or not-for-profit sectors.

Declarations

Competing interests The authors declare no competing interests.

References

1. Florencio-Silva R et al (2015) Biology of bone tissue: structure, function, and factors that influence bone cells. BioMed Res Int. https://doi.org/10.1155/2015/421746
2. Sattary M et al (2022) Polycaprolactone/gelatin/hydroxyapatite nanocomposite scaffold seeded with stem cells from human exfoliated deciduous teeth to enhance bone repair: in vitro and in vivo studies. Mater Technol 37(5):302–315
3. Amini AR et al (2012) Bone tissue engineering: recent advances and challenges. Crit™ Rev Biomed Eng 40(5):363–408
4. Bigham A et al (2021) Zn-substituted Mg2SiO4 nanoparticles-incorporated PCL-silk fibroin composite scaffold: a multifunctional platform towards bone tissue regeneration. Mater Sci Eng C 127:112242
5. Babaei M et al (2022) Effects of low-intensity pulsed ultrasound stimulation on cell seeded 3D hybrid scaffold as a novel strategy for meniscus regeneration: an in vitro study. J Tissue Eng Regen Med 16(9):812–824
6. Baino F et al (2015) Bioceramics and scaffolds: a winning combination for tissue engineering. Front Bioeng Biotechnol 3:202
7. Bramanti P, Mazzon E (2017) The combined strategy of mesenchymal stem cells and tissue-engineered scaffolds for spinal cord injury regeneration. Exp Ther Med 14(4):3355–3368
8. Lyu JS et al (2019) Development of a biodegradable polycaprolactone film incorporated with an antimicrobial agent via an extrusion process. Sci Rep 9(1):1–11
9. Song C et al (2020) Fabrication of PCL scaffolds by supercritical CO2 foaming based on the combined effects of rheological and crystallization properties. Polymers 12(4):780
10. Kazemi M et al (2022) Evaluation of the morphological effects of hydroxyapatite nanoparticles on the rheological properties and printability of hydroxyapatite/polycaprolactone nanocomposite inks and final scaffold features. 3D Print Addit Manuf. https://doi.org/10.1089/3dp.2021.0292

11. Dwivedi R et al (2020) Polycaprolactone as biomaterial for bone scaffolds: review of literature. J Oral Biol Craniofac Res 10(1):381–388
12. Hamlekhan A et al (2010) A proposed fabrication method of novel PCL-GEL-HAp nanocomposite scaffolds for bone tissue engineering applications. Adv Compos Lett 19(4):096369351001900401
13. Ali IH, Ouf A, Elshishiny F, Taskin MB, Song J, Dong M, Chen M, Siam R, Mamdouh W (2022) Antimicrobial and wound-healing activities of graphene-reinforced electrospun chitosan/gelatin nanofibrous nanocomposite scaffolds. ACS Omega 7(2):1838–50
14. Prado-Prone G et al (2020) Single-step, acid-based fabrication of homogeneous gelatin-polycaprolactone fibrillar scaffolds intended for skin tissue engineering. Biomed Mater 15(3):035001
15. Tripathy J (2017) Polymer nanocomposites for biomedical and biotechnology applications. In: Tripathy DK, Sahoo BP (eds) Properties and applications of polymer nanocomposites: clay and carbon based polymer nanocomposites. Springer, Berlin, pp 57–76
16. C. Fernandes *et al.*, "Photodamage and photoprotection: toward safety and sustainability through nanotechnology solutions," in *Food Preservation*: Elsevier, 2017, pp. 527–565.
17. Salehi MH et al (2021) Electrically conductive biocompatible composite aerogel based on nanofibrillated template of bacterial cellulose/polyaniline/nano-clay. Int J Biol Macromol 173:467–480
18. Dey P (2019) Bone mineralization. In: Contemporary topics about phosphorus in biology and materials. Springer, New York
19. Sari M et al (2021) Bioceramic hydroxyapatite-based scaffold with a porous structure using honeycomb as a natural polymeric Porogen for bone tissue engineering. Biomater Res 25(1):1–13
20. Wang C et al (2020) 3D printing of bone tissue engineering scaffolds. Bioact Mater 5(1):82–91
21. Bártolo P et al (2009) Biomanufacturing for tissue engineering: present and future trends. Virtual Phys Prototyp 4(4):203–216
22. Lin K et al (2019) 3D printing of bioceramic scaffolds—barriers to the clinical translation: from promise to reality, and future perspectives. Materials 12(17):2660
23. Ngo TD et al (2018) Additive manufacturing (3D printing): a review of materials, methods, applications and challenges. Composite B 143:172–196
24. Ravi T et al (2020) 3D printed patient specific models from medical imaging-a general workflow. Mater Today 22:1237–1243
25. Jakus AE et al (2016) Hyperelastic "bone": a highly versatile, growth factor–free, osteoregenerative, scalable, and surgically friendly biomaterial. Sci Transl Med 8(358):358ra127
26. Thitiset T et al (2021) A novel gelatin/chitooligosaccharide/demineralized bone matrix composite scaffold and periosteum-derived mesenchymal stem cells for bone tissue engineering. Biomater Res 25(1):1–11
27. Sultana T et al (2017) Preparation and physicochemical characterization of nano-hydroxyapatite based 3D porous scaffold for biomedical application. Adv Tissue Eng Regen Med Open Access 3(3):00065
28. Norouzi M et al (2021) Adipose-derived stem cells growth and proliferation enhancement using poly (lactic-co-glycolic acid)(PLGA)/fibrin nanofiber mats. J Appl Biotechnol Rep 8(4):361–369
29. Kokubo T, Takadama H (2006) How useful is SBF in predicting in vivo bone bioactivity? Biomaterials 27(15):2907–2915
30. Zhou X et al (2019) Biocompatibility and biodegradation properties of polycaprolactone/polydioxanone composite scaffolds prepared by blend or co-electrospinning. J Bioact Compat Polym 34(2):115–130
31. Wandiyanto JV et al (2019) The fate of osteoblast-like MG-63 cells on pre-infected bactericidal nanostructured titanium surfaces. Materials 12(10):1575
32. Karizmeh MS et al (2022) An in vitro and in vivo study of PCL/chitosan electrospun mat on polyurethane/propolis foam as a bilayer wound dressing. Mater Sci Eng 135:112667
33. Amiri F et al (2022) Fabrication and assessment of a novel hybrid scaffold consisted of polyurethane-gellan gum-hyaluronic acid-glucosamine for meniscus tissue engineering. Int J Biol Macromol 203:610–622
34. Chen G, Kawazoe N (2016) Preparation of polymer scaffolds by ice particulate method for tissue engineering. Biomaterials nanoarchitectonics. Elsevier, Amsterdam, pp 77–95
35. Aktug SL et al (2019) Surface and in vitro properties of Ag-deposited antibacterial and bioactive coatings on AZ31 Mg alloy. Surf Coat Technol 375:46–53
36. Leu Alexa R et al (2021) 3D printing of alginate-natural clay hydrogel-based nanocomposites. Gels 7(4):211
37. Abbasi N et al (2020) Porous scaffolds for bone regeneration. J Sci 5(1):1–9
38. Ansari MA, Golebiowska AA, Dash M, Kumar P, Jain PK, Nukavarapu SP, Ramakrishna S, Nanda HS (2022) Engineering biomaterials to 3D-print scaffolds for bone regeneration: practical and theoretical consideration. Biomater Sci 10(11):2789–816
39. Cakmak AM et al (2020) 3D printed polycaprolactone/gelatin/bacterial cellulose/hydroxyapatite composite scaffold for bone tissue engineering. Polymers 12(9):1962
40. Shanthi PMS et al (2009) Synthesis and characterization of nanohydroxyapatite at ambient temperature using cationic surfactant. Mater Lett 63(24–25):2123–2125
41. Yu C et al (2019) Effect of bifunctional montmorillonite on the thermal and tribological properties of polystyrene/montmorillonite nanocomposites. Polymers 11(5):834
42. Raizda P et al (2016) Preparation and photocatalytic activity of hydroxyapatite supported BiOCl nanocomposite for oxytetracyline removal. Adv Mater Lett 7(4):312–318
43. Wlodarczyk D et al (2021) Structural evaluation of percolating, self-healing polyurethane–polycaprolactone blends doped with metallic, ferromagnetic, and modified graphene fillers. Polym Polym Compos 29(5):541–552
44. Varma H, Babu SS (2005) Synthesis of calcium phosphate bioceramics by citrate gel pyrolysis method. Ceram Int 31(1):109–114
45. Yang X et al (2010) The performance of dental pulp stem cells on nanofibrous PCL/gelatin/nHA scaffolds. J Biomed Mater Res Part A 93(1):247–257
46. Jaiswal A et al (2013) Enhanced mechanical strength and biocompatibility of electrospun polycaprolactone-gelatin scaffold with surface deposited nano-hydroxyapatite. Mater Sci Eng, C 33(4):2376–2385
47. Hassan MI, Sultana N (2017) Characterization, drug loading and antibacterial activity of nanohydroxyapatite/polycaprolactone (nHA/PCL) electrospun membrane. 3 Biotech 7(4):1–9
48. Baghbadorani MA et al (2021) A ternary nanocomposite fibrous scaffold composed of poly (ε-caprolactone)/Gelatin/Gehlenite (Ca2Al2SiO7): physical, chemical, and biological properties in vitro. Polym Adv Technol 32(2):582–598
49. Sattary M et al (2018) Incorporation of nanohydroxyapatite and vitamin D3 into electrospun PCL/Gelatin scaffolds: the influence on the physical and chemical properties and cell behavior for bone tissue engineering. Polym Adv Technol 29(1):451–462
50. Khodamoradi N et al (2019) Bacterial cellulose/montmorillonite bionanocomposites prepared by immersion and in-situ methods: structural, mechanical, thermal, swelling and dehydration properties. Cellulose 26(13):7847–7861
51. Li D et al (2022) Progress in montmorillonite functionalized artificial bone scaffolds: intercalation and interlocking nanoenhancement, and controlled drug release. J Nanomater. https://doi.org/10.1155/2022/7900382

52. Shuai C et al (2021) Accelerated degradation of HAP/PLLA bone scaffold by PGA blending facilitates bioactivity and osteoconductivity. Bioact Mater 6(2):490–502
53. Olad A, Azhar FF (2014) The synergetic effect of bioactive ceramic and nanoclay on the properties of chitosan–gelatin/nanohydroxyapatite–montmorillonite scaffold for bone tissue engineering. Ceram Int 40(7):10061–10072
54. Wu M et al (2021) Nanoclay mineral-reinforced macroporous nanocomposite scaffolds for in situ bone regeneration: In vitro and in vivo studies. Mater Des 205:109734
55. Rezapourian M et al (2022) Biomimetic design of implants for long bone critical-sized defects. J Mech Behav Biomed Mater 134:105370
56. Xu W et al (2019) Fabrication and properties of newly developed Ti35Zr28Nb scaffolds fabricated by powder metallurgy for bone-tissue engineering. J Market Res 8(5):3696–3704
57. Liao C et al (2020) Polyetheretherketone and its composites for bone replacement and regeneration. Polymers 12(12):2858
58. Ab Aziz bin Mohd Yusof M et al. The effect of porosity and contact angle on the fluid capillary rise for bone scaffold wettability and absorption
59. Etemadi N et al (2021) Novel bilayer electrospun poly (caprolactone)/silk fibroin/strontium carbonate fibrous nanocomposite membrane for guided bone regeneration. J Appl Polym Sci 138(16):50264
60. Li Y et al (2014) Nanofibers support oligodendrocyte precursor cell growth and function as a neuron-free model for myelination study. Biomacromol 15(1):319–326
61. Zadehnajar P et al (2020) Preparation and characterization of poly ε-caprolactone-gelatin/multi-walled carbon nanotubes electrospun scaffolds for cartilage tissue engineering applications. Int J Polym Mater Polym Biomater 69(5):326–337
62. Nitya G et al (2012) In vitro evaluation of electrospun PCL/nanoclay composite scaffold for bone tissue engineering. J Mater Sci Mater Med 23(7):1749–1761
63. Xia Y et al (2013) Selective laser sintering fabrication of nanohydroxyapatite/poly-ε-caprolactone scaffolds for bone tissue engineering applications. Int J Nanomed 8:4197
64. Rajzer I (2014) Fabrication of bioactive polycaprolactone/hydroxyapatite scaffolds with final bilayer nano-/micro-fibrous structures for tissue engineering application. J Mater Sci 49(16):5799–5807
65. Hadizadeh M et al (2021) A bifunctional electrospun nanocomposite wound dressing containing surfactin and curcumin: In vitro and in vivo studies. Mater Sci Eng C 129:112362
66. Jafari A et al (2020) Bioactive antibacterial bilayer PCL/gelatin nanofibrous scaffold promotes full-thickness wound healing. Int J Pharm 583:119413
67. Zahiri M et al (2020) Encapsulation of curcumin loaded chitosan nanoparticle within poly (ε-caprolactone) and gelatin fiber mat for wound healing and layered dermal reconstitution. Int J Biol Macromol 153:1241–1250
68. Dana K, Sarkar M (2020) Organophilic nature of nanoclay. Clay nanoparticles. Elsevier, Amsterdam, pp 117–138
69. Tao L et al (2017) In vitro and in vivo studies of a gelatin/carboxymethyl chitosan/LAPONITE® composite scaffold for bone tissue engineering. RSC Adv 7(85):54100–54110
70. Mirmusavi MH et al (2019) Evaluation of physical, mechanical and biological properties of poly 3-hydroxybutyrate-chitosan-multiwalled carbon nanotube/silk nano-micro composite scaffold for cartilage tissue engineering applications. Int J Biol Macromol 132:822–835
71. Gaharwar AK et al (2014) Nanoclay-enriched poly (ε-caprolactone) electrospun scaffolds for osteogenic differentiation of human mesenchymal stem cells. Tissue Eng Part A 20(15–16):2088–2101
72. Fathi M et al (2008) Preparation and bioactivity evaluation of bone-like hydroxyapatite nanopowder. J Mater Process Technol 202(1–3):536–542
73. Mousa M et al (2018) Clay nanoparticles for regenerative medicine and biomaterial design: a review of clay bioactivity. Biomaterials 159:204–214
74. Polo-Corrales L et al (2014) Scaffold design for bone regeneration. J Nanosci Nanotechnol 14(1):15–56
75. Mirmusavi MH et al (2022) Polycaprolactone-chitosan/multiwalled carbon nanotube: a highly strengthened electrospun nanocomposite scaffold for cartilage tissue engineering. Int J Biol Macromol 209:1801–1814
76. Boroojen FR et al (2019) The controlled release of dexamethasone sodium phosphate from bioactive electrospun PCL/gelatin nanofiber scaffold. Iran J Pharm Res 18(1):111
77. L. Ghasemi-Mobarakeh, P. Prabhakaran, M. Morshed, M. Nasr-Esfahani MH, Ramakrishna S. Electrospun poly (ε-caprolactone)/gelatin nanofibrous scaffolds for nerve tissue engineering,"*Biomaterials,* vol. 29, pp. 4532-9, 2008.
78. Trakoolwannachai V et al (2019) Characterization of hydroxyapatite from eggshell waste and polycaprolactone (PCL) composite for scaffold material. Composite B 173:106974
79. Hege CS et al (2020) Biopolymer systems in soft tissue engineering: cell compatibility and effect studies including material, catalyst, and surface properties. ACS Appl Polym Mater 2(8):3251–3258
80. Eskandarinia A et al (2020) A propolis enriched polyurethane-hyaluronic acid nanofibrous wound dressing with remarkable antibacterial and wound healing activities. Int J Biol Macromol 149:467–476
81. Hsu S-H et al (2012) Biocompatibility and antimicrobial evaluation of montmorillonite/chitosan nanocomposites. Appl Clay Sci 56:53–62
82. Huang Y et al (2019) Reinforcement of polycaprolactone/chitosan with nanoclay and controlled release of curcumin for wound dressing. ACS Omega 4(27):22292–22301
83. Jamshidi M et al (2019) Nanoclay reinforced starch-polycaprolactone scaffolds for bone tissue engineering. J Tissues Mater 2(1):55–63
84. Maisanaba S et al (2014) In vivo toxicity evaluation of the migration extract of an organomodified clay–poly (lactic) acid nanocomposite. J Toxicol Environ Health A 77(13):731–746
85. Estandarte AK et al (2016) The use of DAPI fluorescence lifetime imaging for investigating chromatin condensation in human chromosomes. Sci Rep 6(1):1–12
86. Hoang QQ et al (2003) Bone recognition mechanism of porcine osteocalcin from crystal structure. Nature 425(6961):977–980
87. Mieszawska AJ et al (2011) Clay enriched silk biomaterials for bone formation. Acta Biomater 7(8):3036–3041
88. Sato M et al (2008) Nanocrystalline hydroxyapatite/titania coatings on titanium improves osteoblast adhesion. J Biomed Mater Res Part A 84(1):265–272
89. Hynes RO (2002) Integrins: bidirectional, allosteric signaling machines. Cell 110(6):673–687